ARTICLE

Tuning the Dielectric Response of Water in Nanoconfinement through Surface Wettability

Ermioni Papadopoulou, Julija Zavadlav,* Rudolf Podgornik, Matej Praprotnik, and Petros Koumoutsakos

Cite This: *ACS Nano* 2021, 15, 20311−20318

Read Online

ACCESS | Metrics & More | Article Recommendations | SI Supporting Information

ABSTRACT: The tunable polarity of water can be exploited in emerging technologies including catalysis, gas storage, and green chemistry. Recent experimental and theoretical studies have shown that water can be rendered into an effectively apolar solvent under nanoconfinement. We furthermore demonstrate, through molecular simulations, that the static dielectric constant of water can be modified by changing the wettability of the confining material. We find the out-of-plane dielectric response to be highly sensitive to the level of confinement and can be reduced up to 40×, in accordance with experimental data. By altering the surface wettability from superhydrophilic to superhydrophobic, we observe a 36% increase for the out-of-plane and a 31% decrease for the in-plane dielectric constants. Our findings demonstrate the feasibility of tunable water polarity, a phenomenon with great potential for scientific and technological impact.
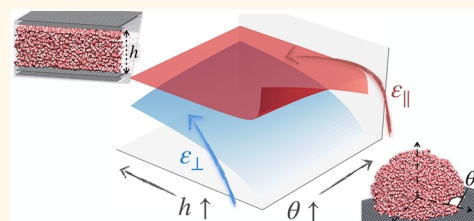
KEYWORDS: *dielectric constant, confined water, molecular dynamics, surface wettability, surface tuning*

The behavior of water at surfaces and interfaces[1−9] is critical to the structure, stability, flexibility, and dynamics of biological macromolecules such as lipid membranes,[10] nucleic acids,[11] proteins,[12] and their complexes, enabling their proper functionality.[13] Dielectric properties of water in contact and/or confined between soft or hard, hydrophobic or hydrophilic bounding surfaces, are particularly important also in the context of long-range interactions in biological systems,[14] since both quintessential components of the nanoscale long-range interactions,[15] the van der Waals interaction[16] as well as the electric double-layer interactions,[17] depend crucially on the static as well as dynamic dielectric response of the media involved. Despite its well-established importance, the experimental probing of the dielectric response of interfacial water has been limited. However, in a recent feat of nanoscale experimentation, Fumagalli *et al.*[18] measured the local capacitance of water layers, confined between two atomically flat graphite crystal surfaces at nanometer separations. They reported an interfacial layer with an anomalously low out-of-plane dielectric constant ($\varepsilon_\perp \approx 2$). These findings have been confirmed by several studies employing molecular dynamics (MD) simulations.[19−29] Decreased $\varepsilon_\perp$ was observed in various confining geometries,[22] for protic (capable of hydrogen bonding) and aprotic fluids,[27] whereas the phonons[6] of the graphene sheets have not been linked to variations of static dielectric water properties.[26] The anomalous dielectric response was attributed to the orientation anisotropy of the vicinal water molecules to the channel wall, suppressing the reorientation of polarization.[21,23,27]

The structural and dynamical behavior of the interfacial water layer is known to depend on the chemical composition of the confining material, that is, on the interactions between the channel and water atoms, which can be characterized by the surface wettability.[2] Optical techniques have introduced the water contact angle θ as the experimentally determinable metric that quantifies the wettability of a surface,[30] with θ values lower than 90° denoting a hydrophilic surface and θ values higher than 90° denoting a hydrophobic surface. Thus, apart from adjusting the level of confinement, dielectric properties could also be tuned by selecting the confining material. For example, the wettability of the graphene can be altered with substrates due to its wetting transparency and can be even reversibly modulated with external stimulation.[31] Techniques that can tune the graphene surface wettability are currently being considered for different nanotechnology applications[31,32] such as self-cleaning, water harvesting, and various nanofluidic devices. Interestingly, previous computational investigations into dielectric response of confined water did not consider the wettability aspect or have reported only the in-plane dielectric response for selected cases.[19,20]
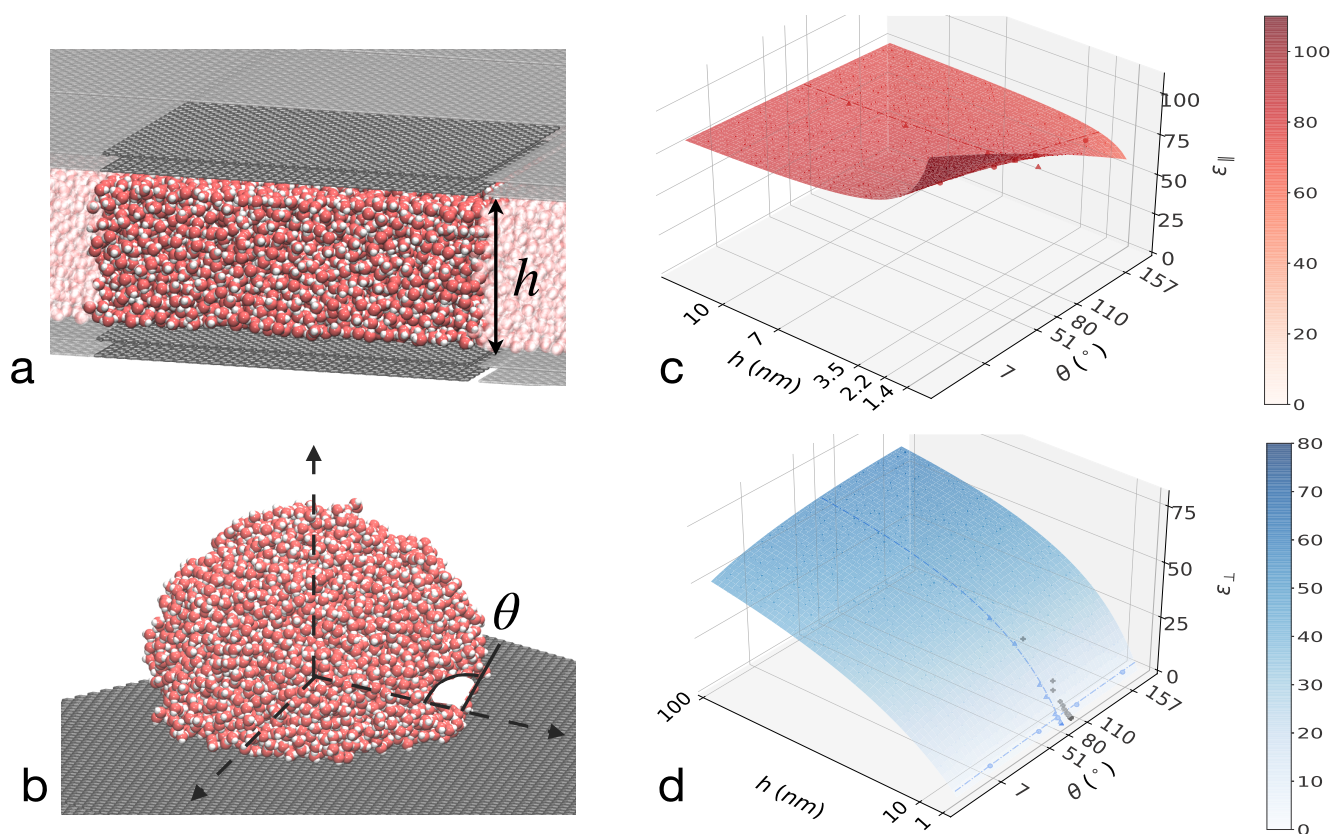
Figure 1. (a) Schematic representation of the simulated channel confined water with the periodic images shown in transparent. (b) Different surface wettabilities measured by the corresponding contact angles θ. (c,d) Surface plots of $\varepsilon_\parallel$ and $\varepsilon_\perp$ with respect to the height of the confinement h and the surface channel wettability measured by the contact angle θ. The colored points correspond to simulation results and gray markers (setting $\theta = 90°$) to previous experimental results.[18]

RESULTS AND DISCUSSION

Here, we employ extensive atomistic MD simulations to characterize the dielectric response of water in planar nanoconfinement. We report the in-plane and out-of-plane dielectric components for various heights of confinement as well as different surface wettabilities of the channel walls. We find that the out-of-plane dielectric component exceedingly decreases as the height of the confinement decreases, whereas it increases as the surface wettability changes from hydrophilic to hydrophobic. We report the opposite trends for the in-plane dielectric constant, although the increase of the parallel component with decreasing channel height is moderate and evident only for confinements smaller than $\approx$10 nm. We rationalize the dielectric response of confined water by investigating the structural changes of water at the interface, with the use of local order parameters, which are metrics for the tetrahedrality and dipole orientation of the confined water. Additionally, we augment the capacitance model[18,33,34] with the simulation extracted interfacial layer properties and propose a two-dimensional (2D) response surface of in-plane and out-of-plane dielectric constants with respect to the channel height and the surface wettability. The constructed phenomenological model enables the prediction of the static dielectric response beyond the simulated channels.

RESULTS AND DISCUSSION

The static dielectric response and the nonbulk-like structural properties of the nanoconfined water are investigated for various channel heights h as well as different surface

wettabilities of the channel walls, denoted through the corresponding water contact angle θ (Figure 1a,b).

To be able to directly compare with experimental results,[18] we explore 10 channel heights with h ranging between 0.5 and 30 nm. These simulations are performed at a fixed channel surface wettability ($\theta = 80°$), which roughly corresponds to a pure graphene surface.[31] The effect of the surface wettability is probed at a fixed channel height ($h = 2.2$ nm) using five wettability-varying surfaces (θ varied between 7° and 157°). We, thus, probe a wide spectrum of confining surfaces, ranging from superhydrophilic to superhydrophobic.

Static Dielectric Response. In the bulk, the dielectric constant of water is isotropic and can be computed *via* fluctuations of the total dipole moment and the Clausius−Mosotti relation[35−37] (Supporting Information). In our simulations, we obtain the value of $\varepsilon = 80.25 \pm 0.65$, which within error bars matches the reported value of $\varepsilon = 79.63$ for the employed SPC/Fw model.[38] In confinement, the dielectric response is anisotropic, and the component of the second-rank tensor exhibits spatial inhomogeneity.[19,39−41] For planar confinements, the dielectric response profile can be fully characterized by the parallel ($\parallel$, in-plane) and normal ($\perp$, out-of-plane) components of the dielectric constant with respect to the surface of confinement. In distinction to some previous studies,[21,23] our simulations are performed under no external field. Instead, dielectric response is extracted from the equilibrium simulations using the framework proposed by Ballenegger *et al.*[19,39,41] (described in detail in Supporting Information).
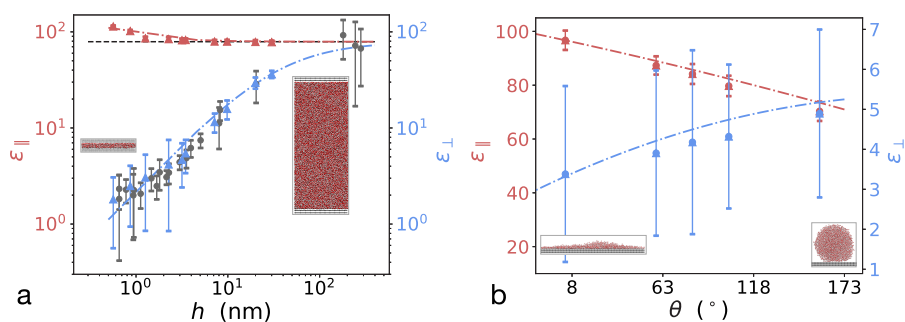
Figure 2. Dielectric response of water in confinement for various (a) heights and (b) surface wettabilities. The effective normal $\varepsilon_\perp$ (blue) and effective parallel $\varepsilon_\parallel$ (red) components of the dielectric constant of water are calculated along the whole height of the confinement. The red and blue dashed-dotted lines correspond to the 2D capacitance model prediction (eqs 1 and 2) for $\theta = 80°$ in (a) and for $h = 2.2$ nm in (b). The error bars denote the standard deviation. (a) Results are compared with the experimental data[18] (gray points). Bulk value of the dielectric constant of water is denoted with the dashed black line.
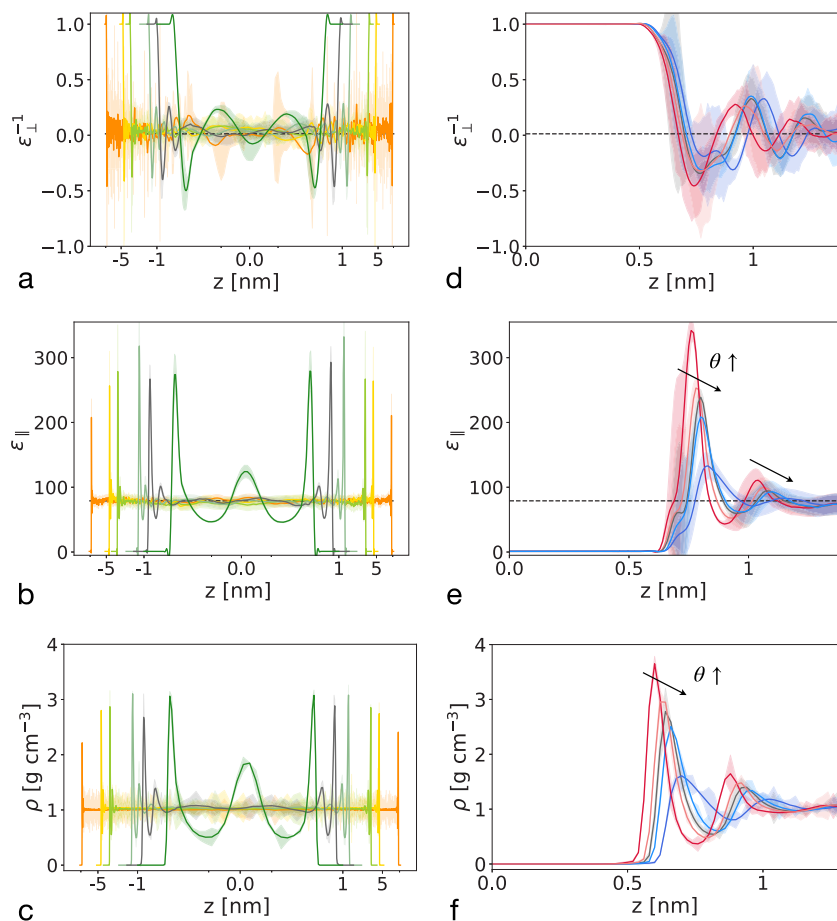
Figure 3. Spatial distribution of the inverse normal dielectric constant $\varepsilon_\perp^{-1}$. (a,d) Parallel dielectric constant $\varepsilon_\parallel$ (b,e) and density (c,f) with standard deviations (shaded regions). The x-axis for (a–c) is in symmetric logarithmic scale with $z = 0$ denoting the middle of the channel, while for (d–f) $z = 0$ denotes the start point of the graphene wall. (a–c) The green, gray, light green, gold, and orange curves correspond to the channel heights of $h = 1.4, 2.2, 7, 10, 20$ nm, respectively. (d–f) The red, light red, gray, light blue, and blue curves correspond to contact angles of 7, 52, 80, 110, 157°.

At a fixed wettability, we observe a drastic decrease in the perpendicular dielectric constant as the height of the channel is decreased (Figure 2, exact values in Table S2).

The obtained values, calculated along the overall height of the confinement, are in excellent agreement with the experimental data reported by Fumagalli *et al.*[18] In comparison, the reported values in a recent MD study[24] somewhat underestimate the dielectric constant. Discrepancies between the experimental and simulation results as well as between different simulations can be attributed to the various employed water models and wettability of the surface.[31] The normal dielectric constant attains the bulk value only for channel heights larger than ≈ 100 nm. On the other hand, the effective parallel component of the dielectric constant of water is found to increase for confinements below ≈ 10 nm. However, deviations from the bulk values are smaller compared to the
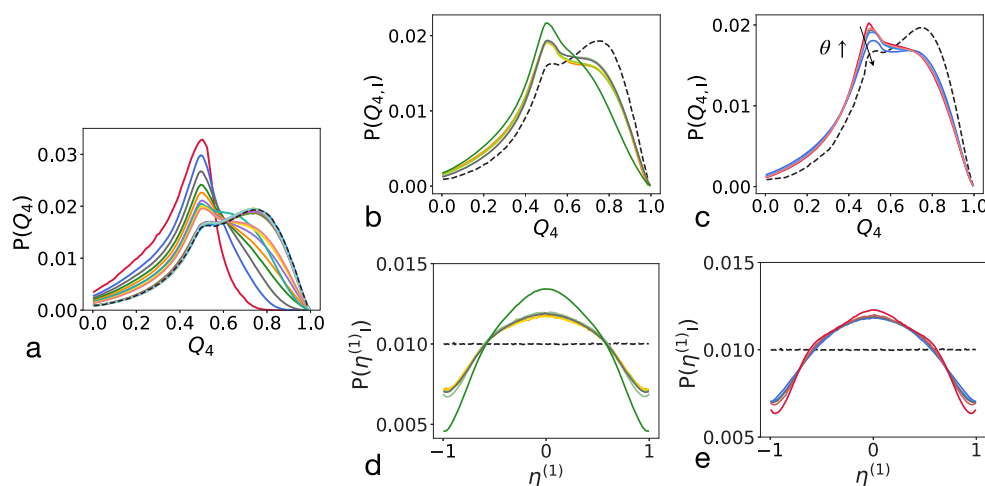
Figure 4. Distribution of Q_4 (a−c) and $\eta^{(1)}$ (d−e) order parameters. (a) The red, blue, gray, green, orange, purple, sea-green, gold, rose, light blue, olive green, magenta, khaki, light red, yellow green, and sky blue curves are computed for slabs of 0.1 nm thickness at increased distance (from 0.2 to 1 nm) from the channel wall. The profiles are shown for channel height h = 3.5 nm. (b−e) Distribution in the interface layer (within 0.9 nm from the channel wall) for contact angle θ = 80° and heights h = 1.4, 2.2, 3.5, 7, 10, and 20 nm shown in green, gray, sea green, light green, gold and orange, respectively (b,d) and for height h = 2.2 nm and contact angles of θ = 7, 52, 80, 110, and 157° shown in red, light red, gray, light blue and blue, respectively (c,e). The black dashed curves correspond to the distributions of bulk, unconfined water.

normal component. For the smallest considered channel height (h = 0.5 nm), the increase is around 40%. An increase in the parallel dielectric response was reported also in the previous studies. Nonetheless, it remains unresolved, as results are quantitatively in disagreement. Hamid et al.[42] report a more pronounced increase of $\varepsilon_{\parallel}$, which deviates from the bulk value for channel heights up to ≈100 nm. Schlaich et al.,[41] in contrast, report for soft polar surface confinement only a slight increase (≈ 10%) but only for channel heights below ≈0.5 nm. We note that quantitatively the results also depend on the calculation of $\varepsilon_{\parallel}$ (Supporting Information). Typically effective values are reported. If $\varepsilon_{\parallel}$ is instead computed as an average over the spatial distribution profile, then lower values are obtained (Figure S2).

Next, we fix the channel height and examine the impact of surface wettability of the channel walls. Interestingly, we find that both components of the dielectric constant are affected, but that these effects are smaller than the effect of the channel height as well as that they act oppositely for the two components. Upon modifying the wettability from hydrophilic to hydrophobic (θ ↑), the normal dielectric constant is increased by 36%, whereas the parallel component is decreased by 31%. These percentages are calculated as the difference between the most hydrophilic and most hydrophobic tested surfaces, divided by the value obtained for the roughly neutral surface (θ = 80°). Insight for the observed behavior can be obtained by looking at the dielectric profiles along the channel height.

For the inverse normal dielectric response (Figure 3a,d), we observe an overscreening behavior in the interface layer, consistent with previous work.[19] The response profile of $\varepsilon_{\perp}$ (Figure S1) displays numerous infinite discontinuities (at $\varepsilon_{\perp}^{-1}$ = 0) and regions with negative values giving rise to low values of normal dielectric constant in the proximity of the wall surfaces. The observed reduction of overall $\varepsilon_{\perp}$ with the decrease of the channel height can be roughly understood in terms of the proportionality between the interface and the bulk regions. The $\varepsilon_{\perp}$ dependency on surface wettability can be traced back to the charge density profile along the channel height (Figure

S1) from which the perpendicular response is extracted. As the wettability of the confining surface is reduced (θ ↑), the charge density profile becomes smoother. This translates into an increase of $\varepsilon_{\perp}$.

The parallel component of the dielectric profile (Figure 3b,e) is well correlated with the density distribution inside the channel (Figure 3c,f). In the vicinity of the channel walls, the density profile exhibits several peaks due to the well-known layering of water near the confining boundaries, whereas away from the boundaries, the densities of all channels collapse to the expected bulk density value.[43,44] The density peak positions and values are independent of the channel height variation (Figure 3c). An exception from this behavior are channels with h < 2 nm, where water does not exhibit a distinct bulk-like region in the middle of the channel. On the other hand, the variation of the surface wettability induces changes in the density profile near the channel walls (Figure 3f). Going from hydrophilic to hydrophobic surfaces (θ ↑), the layering becomes less and less pronounced. The water molecules are pushed away from the walls, as evident from the shifted water density peaks toward the channel interior. The same behavior is observed for the dielectric response in the parallel direction and is consequently reflected in the overall $\varepsilon_{\parallel}$, which decreases as we move from hydrophilic to hydrophobic (θ ↑) channel walls. Bonthuis et al.[19] retrieved a reverse correlation between $\varepsilon_{\parallel}$ and density. We believe that this observation is related to the fact that the water volume was not confined in a channel and that the variation of the surface wettability was performed with a chemical deposition of terminal ion groups on the surface. We note that in a recent study by Kwon et al.,[45] an increased value of contact angle was connected to a decrease of density and the relative permittivity, in accordance with our results.

We also examined the total average water density inside channels to ensure that the water in each channel is well equilibrated. For channel heights above h = 2 nm, we find that the confined water density values agree with the unconfined water density of 1.01 g/cm^3 (ref 38 and our simulations) at ambient conditions (exact values in Table S1). An increased
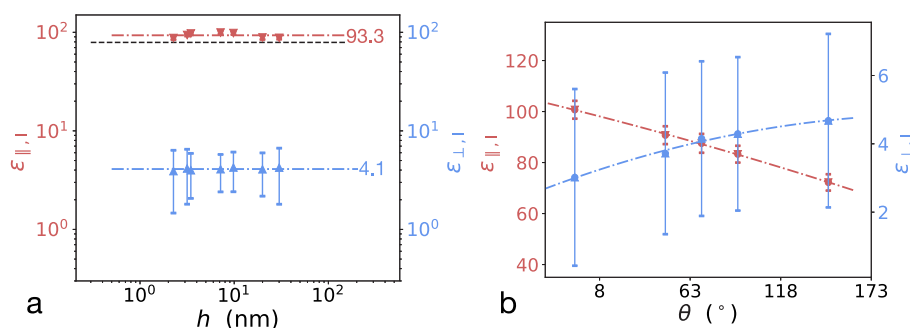
Figure 5. Normal $\varepsilon_{\perp,\mathrm{I}}$ (blue) and parallel $\varepsilon_{\parallel,\mathrm{I}}$ (red) components of the dielectric constant of water computed in the interface region for various (a) heights and (b) surface wettabilities. The error bars denote the standard deviation. (a) The red and blue dashed lines correspond to the average values of $\varepsilon_{\perp,\mathrm{I}}$ and $\varepsilon_{\parallel,\mathrm{I}}$. Bulk value of the dielectric constant of water is denoted with the black dashed line. (b) The red and blue dashed lines correspond to the fitted relation between the interface dielectric constnat and surface wettability (Supporting Information).

density is found for very small channels, which is reasonable since at such small separations, water never reaches the bulk behavior as already stated before. Similar density deviations were also observed in other studies.[4,26]

Characterizing the Interface Layer. As the variations in the density as well as in the dielectric response are located in the interface region near the channel walls, we determine the extent of the region where water exhibits nonbulk-like behavior by examining several of its local order parameters: (i) the dipole moment orientation $\eta^{(1)}$, (ii) the nematic order $\eta^{(2)}$, (iii) the quadrupole moment in direction of the channel height $\eta^{(3)}$, and the tetrahedrality $Q_4(z)$ (defined in Supporting Information). Computing the average order parameters *vs* distance from the channel walls (Figure S4), we observe that (irrespective of h and θ) in close proximity to the walls, all order parameters showcase a structure that differs from the bulk and only approach bulk values at distances ≈ 0.9 nm from the wall.

To determine a more precise value for the height of the interface layer h_I, we perform a sensitivity study for the distribution of Q_4 order parameter (Figure 4a).

In particular, the distribution is probed in thin regions centered at various distances from the channel wall. We focus on the tetrahedral order parameter due to its connection with the hydrogen-bond network of water. Q_4 can take values between 0 and 1, with the former characterizing the random distribution and the latter corresponding to the regular tetrahedral symmetry. At ambient conditions, the average tetrahedrality of water in bulk is $Q_4 \approx 0.6$.[46] With increased distance from the channel surface, the distribution of Q_4 shifts from a unimodal to a bimodal distribution and progressively resembles the bulk distribution. Beyond 0.9 nm, the distributions collapse to the bulk distribution. Repeating this analysis for different channel heights and wettabilities, we find that h_I is not affected by neither (Figure S6).

With the height of the interface layer set to $h_\mathrm{I} = 0.9$ nm, we then compute the tetrahedrality distribution in the interface layer $Q_{4,\mathrm{I}}$ (Figure 4b,c). For very small channel heights ($h < 2$ nm), the distribution is very distinct from the other cases, denoting a structure highly affected by the interface. As already mentioned, the separation between channel walls is so small that no bulk-like region is formed and the distribution is computed in the whole channel since $h < 2h_\mathrm{I}$. For all other channel heights, the $P(Q_{4,\mathrm{I}})$ are approximately equal (see also Figure S4). In contrast, a clear sequence of distribution profiles can be seen for different wettability cases (Figure 4c). Upon

altering the channel material from hydrophilic to hydrophobic ($\theta \uparrow$), the first peak in the distribution decreases and approaches values of the unconfined water. These results demonstrate that water in proximity to hydrophilic surfaces tends to interact with the surface and the hydrogen-bond network is highly perturbed.

Similar conclusions can be deduced from the dipole moment distributions $P(\eta^{(1)})$ of water molecules in the interface layer (Figure 4d,e). In the bulk, the water dipole moments have no preferred orientation in space and thus the mean value of $\eta^{(1)} = 0$, while $P(\eta^{(1)})$ is constant for all $\eta^{(1)}$. In the interface region, a preferred orientation of water molecules is evident. Irrespective of the material surface, the highest probability is found at $\eta^{(1)} = 0$, which corresponds to dipole moments lying in the plane parallel to the wall. However, this preferred orientation appears more pronounced the more hydrophilic the channel material. To verify the correct determination of h_I, we also calculate $P(Q_4)$ and $P(\eta^{(1)})$ in the bulk-like region of the channel, that is, the region excluding the two interface layers (Figure S5). We find all profiles to match well with the unconfined water results.

2D Capacitance Model. Since the structural characteristics in the interface layer hinge on the wettability of the confining material but not on the height of the confinement, we expect a complementary dependency for the dielectric constant in the interface layer. Figure 5 shows that this is indeed the case.

The results are used to build a phenomenological capacitance model in order to predict the dielectric constant of nanoconfined water beyond the simulated cases. To this end, we extend the previously proposed capacitance model[18,33,34] to include the wettability effects. The effective overall $\varepsilon_\perp$ and $\varepsilon_\parallel$ can be obtained by considering the two interface layer capacitors and the bulk capacitor connected in series and in parallel, respectively. Furthermore, by considering the interface layer capacitors as wettability dependent, we obtain the following relations:

$$\varepsilon_\perp(h, \theta) = \frac{h}{\frac{2h_\mathrm{I}}{\varepsilon_{\perp,\mathrm{I}}(\theta)} + \frac{h - 2h_\mathrm{I}}{\varepsilon_\mathrm{B}}} \qquad (1)$$

and

$$\varepsilon_\parallel(h, \theta) = \frac{2h_\mathrm{I}}{h}\varepsilon_{\parallel,\mathrm{I}}(\theta) + \frac{h - 2h_\mathrm{I}}{h}\varepsilon_\mathrm{B} \qquad (2)$$

where $\varepsilon_{\perp,I}(\theta)$ and $\varepsilon_{\parallel,I}(\theta)$ relations are extracted from Figure 5b (Supporting Information), h_I = 0.9 nm as determined above, and ε_B = 79 the bulk dielectric constant of water. The obtained 2D surface plots of dielectric response of water with respect to the height of the confinement and the wettability of the channel wall (Figure 1c,d) match well the experimental as well as simulation data. Both components of the dielectric response are affected under the confinement and depend also on the wettability of the confining material. In comparison to the degree of confinement, that is, h, the consequences of wettability are not as drastic but still considerable, especially for small h.

CONCLUSIONS

In summary, we have demonstrated the possibility of tuning the dielectric response of water in nanoconfinement through modifications of the surface wettability. The present computational study investigates the interdependency of the confinement size with the wettability properties of the confining surfaces. Our results demonstrate that the abnormal dielectric response of water in planar confinement is due to the nonbulk-like behavior of the interfacial water. The structural characteristics in the interfacial layer are sensitive to the hydrophilic/hydrophobic nature of the confining wall material and consequently play a role also in the overall dielectric response. Aside from the level of confinement, the wettability can therefore serve as an additional fine-tuning parameter for the manipulation of dielectric response of water. To obtain a low dielectric constant of the solvent, our results advocate for a small confinement size (small h) and a hydrophobic surface material (large θ). We envision that the capability of controlling the 2D response of the water dielectric constant could boost critical technologies, such as chemical reactions or gas dissolution that require a lower dielectric constant of the solvent.[47]

METHODS

All simulations are performed with LAMMPS package.[48] We use the velocity Verlet integration with the time step of 1 fs. The cutoff radius for the nonbonded interactions is 3σ, where σ is the largest Lennard-Jones (LJ) interaction parameter (σ_{CO} = 0.319 nm) in the system. The electrostatic interactions beyond the cutoff are corrected with the particle−particle particle-mesh (P3M) solver scheme[49] with a root-mean-squared error in the force calculation of 10^{-5}. In the z-direction, we exclude the long-ranged electrostatic contributions from the periodic images, introducing the correction for slab geometry.[50] The slab-geometry correction resembles the computation of the 2D Ewald summation on a simulation system with a finite length along the third dimension.[27,50] The temperature of 298 K is maintained in the NVT ensemble with the Nosé−Hoover thermostat with the constant of τ_T = 0.1 ps.

Water is modeled with SPC/Fw[38] model, as it reproduces well the bulk dielectric constant of water. The wall atoms remain fixed for all simulations, in order to omit effects due to phonon excitations.[6] The surface wettability is controlled by modifying the energetic parameters of the nonbonded interaction between the graphitic surface and water. In particular, the interaction is modeled with the LJ potential with σ_{CO} = 0.319 nm. Several depths of the potential well are considered ϵ_{CO} = 0.16369, 0.11369, 0.09369, 0.07369, 0.02369 kcal/mol, which, respectively correspond to the following water (SPC/Fw) contact angles on a flat graphene surface: θ = 7, 52, 80, 110, and 157°. These contact angles are determined from separate simulations of water droplets on planar surfaces, and computation follows the method introduced in Werder et al.[51] For simulations with channel height variations, the contact angle is set to θ = 80°, that is, roughly

corresponding to the pure graphene surface.[31] Determining the wettability of flat graphene has been a source of controversy among experimental studies, since the measured contact angles of water deposited on graphene reported in the literature vary from neutral wettability values ($\sim$90°)[52−55] to more hydrophilic values,[56,57] with these discrepancies being attributed to airborne contamination of experimental samples.[57]

The nanochannels are constructed using two graphene-like layers with the WCCNT package.[58] The width and length of the channels are set to l_x, $l_y \approx$ 10 nm, while the height of the channel h varies for different setups. We simulate 10 systems with h = 0.5, 0.8, 1.4, 2.2, 3.0, 3.5, 7.0, 10, 20, and 30 nm. We use periodic boundary conditions in the planar directions and nonperiodic boundary conditions in the normal directions of the channel, where the slab correction is applied for the computation of long-range electrostatics, by adding a vacuum space of 3× the slab height in between periodic images.

The protocol for the simulations consists of two phases: equilibration and production runs. The systems used for the equilibration runs consist of a nonperiodic channel with water reservoirs placed in both ends of the channel. A constant force is applied to all water molecules at the outer edges of the reservoirs, pushing the water in the channel until the density within the channels is equilibrated. The value of the force is selected so that the sum of forces applied to all water molecules normalized with the cross-sectional area corresponds to a pressure of 1 bar. After equilibration, the reservoirs are removed and periodic boundaries are applied. The production runs are performed for a total of 40 ns for all smaller systems and for 30 ns for channel sizes above 7 nm. The trajectories of the water molecules are saved every 0.5 ps. The analysis of the trajectories takes place after the first 1 ns of the production run simulation. Visualizations were performed with the Visual Molecular Dynamics (VMD) package.[59]

ASSOCIATED CONTENT

Ⓢ **Supporting Information**

The Supporting Information is available free of charge at https://pubs.acs.org/doi/10.1021/acsnano.1c08512.

> Additional MD simulation details, density computation, total density of confined water, dielectric constant computation, charge density profiles, perpendicular dielectric response profiles, order parameters definitions and profiles, and order parameters distributions (PDF)

AUTHOR INFORMATION

Corresponding Author

Julija Zavadlav − *Professorship of Multiscale Modeling of Fluid Materials, TUM School of Engineering and Design, Technical University of Munich, DE-85748 Garching near Munich, Germany;* ⓘ orcid.org/0000-0002-4495-9956; Email: julija.zavadlav@tum.de

Authors

Ermioni Papadopoulou − *Computational Science and Engineering Laboratory, ETH-Zurich, CH-8092 Zurich, Switzerland*

Rudolf Podgornik − *School of Physical Sciences and Kavli Institute for Theoretical Sciences, University of Chinese Academy of Sciences, Beijing 100049, China; CAS Key Laboratory of Soft Matter Physics, Institute of Physics, Chinese Academy of Sciences, Beijing 100190, China; Wenzhou Institute of the University of Chinese Academy of Sciences, Wenzhou, Zhejiang 325000, China; Department of Physics, Faculty of Mathematics and Physics, University of Ljubljana, SI-1000 Ljubljana, Slovenia*

Matej Praprotnik − *Laboratory for Molecular Modeling, National Institute of Chemistry, SI-1001 Ljubljana, Slovenia;*

Department of Physics, Faculty of Mathematics and Physics, University of Ljubljana, SI-1000 Ljubljana, Slovenia;
ⓘ orcid.org/0000-0003-0825-1659

Petros Koumoutsakos − *Computational Science and Engineering Laboratory, ETH-Zurich, CH-8092 Zurich, Switzerland; John A. Paulson School of Engineering and Applied Sciences, Harvard University, Cambridge, Massachusetts 02138, United States*

Complete contact information is available at:
https://pubs.acs.org/10.1021/acsnano.1c08512

Author Contributions

E.P., J.Z., R.P., M.P., and P.K. designed the study and the MD campaign. E.P. performed the MD simulations and the analysis of the MD results. J.Z. coordinated the project and the analysis of the MD results. R.P, M.P., and P.K. coordinated the project and participated in the discussion of the results. All authors contributed to the writing and editing of the manuscript.

Notes

The authors declare no competing financial interest.

REFERENCES

(1) Gonella, G.; Backus, E. H. G.; Nagata, Y.; Bonthuis, D. J.; Loche, P.; Schlaich, A.; Netz, R. R.; Kuhnle, A.; McCrum, I. T.; Koper, M. T. M.; Wolf, M.; Winter, B.; Meijer, G.; Campen, R. K.; Bonn, M. Kramer Campen, R.; Bonn, M. Water at Charged Interfaces. *Nat. Rev. Chem.* **2021**, *5*, 466−485.

(2) Björneholm, O.; Hansen, M. H.; Hodgson, A.; Liu, L.-M.; Limmer, D. T.; Michaelides, A.; Pedevilla, P.; Rossmeisl, J.; Shen, H.; Tocci, G.; Tyrode, E.; Walz, M.-M.; Werner, J.; Bluhm, H. Water at Interfaces. *Chem. Rev.* **2016**, *116*, 7698−7726.

(3) Calero, C.; Franzese, G. Water under Extreme Confinement in Graphene: Oscillatory Dynamics, Structure, and Hydration Pressure explained as a Function of the Confinement Width. *J. Mol. Liq.* **2020**, *317*, 114027.

(4) Ruiz-Barragan, S.; Muñoz-Santiburcio, D.; Marx, D. Nano-confined Water within Graphene Slit Pores Adopts Distinct Confinement-Dependent Regimes. *J. Phys. Chem. Lett.* **2019**, *10*, 329−334.

(5) Knight, A. W.; Kalugin, N. G.; Coker, E.; Ilgen, A. G. Water Properties under Nano-Scale Confinement. *Sci. Rep.* **2019**, *9*, 8246.

(6) Cruz-Chu, E. R.; Papadopoulou, E.; Walther, J. H.; Popadić, A.; Li, G.; Praprotnik, M.; Koumoutsakos, P. On Phonons and Water Flow Enhancement in Carbon Nanotubes. *Nat. Nanotechnol.* **2017**, *12*, 1106−1108.

(7) Popadić, A.; Praprotnik, M.; Koumoutsakos, P.; Walther, J. H. Continuum Simulations of Water Flow past Fullerene Molecules. *Eur. Phys. J.: Spec. Top.* **2015**, *224*, 2321−2330.

(8) Walther, J. H.; Praprotnik, M.; Kotsalis, E. M.; Koumoutsakos, P. Multiscale Simulation of Water Flow past a C540 Fullerene. *J. Comput. Phys.* **2012**, *231*, 2677−2681.

(9) Shaat, M.; Javed, U.; Faroughi, S. Wettability and Confinement Size Effects on Stability of Water Conveying Nanotubes. *Sci. Rep.* **2020**, *10*, 17167.

(10) Kanduč, M.; Schneck, E.; Netz, R. R. Hydration Interaction between Phospholipid Membranes: Insight into Different Measure-ment Ensembles from Atomistic Molecular Dynamics Simulations. *Langmuir* **2013**, *29*, 9126−9137.

(11) Zavadlav, J.; Podgornik, R.; Praprotnik, M. Order and Interactions in DNA Arrays: Multiscale Molecular Dynamics Simulation. *Sci. Rep.* **2017**, *7*, 4775.

(12) Ball, P. Water is an Active Matrix of Life for Cell and Molecular Biology. *Proc. Natl. Acad. Sci. U. S. A.* **2017**, *114*, 13327−13335.

(13) Privalov, P.; Crane-Robinson, C. Role of Water in the Formation of Macromolecular Structures. *Eur. Biophys. J.* **2017**, *46*, 203−224.

(14) Kanduc, M.; Schlaich, A.; Schneck, E.; Netz, R. R. Water-Mediated Interactions between Hydrophilic and Hydrophobic Surfaces. *Langmuir* **2016**, *32*, 8767−8782.

(15) French, R. H.; Parsegian, V. A.; Podgornik, R.; Rajter, R. F.; Jagota, A.; Luo, J.; Asthagiri, D.; Chaudhury, M. K.; Chiang, Y.; Granick, S.; Kalinin, S.; Kardar, M.; Kjellander, R.; Langreth, D. C.; Lewis, J.; Lustig, S.; Wesolowski, D.; Wettlaufer, J. S.; Ching, W.; Finnis, M.; et al. Long Range Interactions in Nanoscale Science. *Rev. Mod. Phys.* **2010**, *82*, 1887.

(16) Woods, L. M.; Dalvit, D. A. R.; Tkatchenko, A.; Rodriguez-Lopez, P.; Rodriguez, A. W.; Podgornik, R. Materials Perspective on Casimir and van der Waals Interactions. *Rev. Mod. Phys.* **2016**, *88*, 045003.

(17) Markovich, T.; Andelman, D.; Podgornik, R.; Podgornik, R. In *Handbook of Lipid Membranes: Molecular, Functional, and Materials Aspects*; Safinya, C. R., Rädler, J. O., Eds.; CRC Press: Boca Raton, FL, 2021.

(18) Fumagalli, L.; Esfandiar, A.; Fabregas, R.; Hu, S.; Ares, P.; Janardanan, A.; Yang, Q.; Radha, B.; Taniguchi, T.; Watanabe, K.; Gomila, G.; Novoselov, K. S.; Geim, A. K. Anomalously Low Dielectric Constant of Confined Water. *Science* **2018**, *360*, 1339−1342.

(19) Bonthuis, D. J.; Gekle, S.; Netz, R. R. Dielectric Profile of Interfacial Water and Its Effect on Double-Layer Capacitance. *Phys. Rev. Lett.* **2011**, *107*, 166102.

(20) Gekle, S.; Netz, R. R. Anisotropy in the Dielectric Spectrum of Hydration Water and Its Relation to Water Dynamics. *J. Chem. Phys.* **2012**, *137*, 104704.

(21) De Luca, S.; Kannam, S. K.; Todd, B. D.; Frascoli, F.; Hansen, J. S.; Daivis, P. J. Effects of Confinement on the Dielectric Response of Water Extends up to Mesoscale Dimensions. *Langmuir* **2016**, *32*, 4765−4773.

(22) Schaaf, C.; Gekle, S. Spatially Resolved Dielectric Constant of Confined Water and Its Connection to the Non-Local Nature of Bulk Water. *J. Chem. Phys.* **2016**, *145*, 084901.

(23) Varghese, S.; Kannam, S. K.; Hansen, J. S.; Sathian, S. P. Effect of Hydrogen Bonds on the Dielectric Properties of Interfacial Water. *Langmuir* **2019**, *35*, 8159−8166.

(24) Ahmadabadi, I.; Esfandiar, A.; Hassanali, A.; Ejtehadi, M. R. Structural and Dynamical Fingerprints of the Anomalous Dielectric Properties of Water under Confinement. *Phys. Rev. Materials* **2021**, *5*, 024008.

(25) Jalali, H.; Ghorbanfekr, H.; Hamid, I.; Neek-Amal, M.; Rashidi, R.; Peeters, F. M. Out-of-Plane Permittivity of Confined Water. *Phys. Rev. E: Stat. Phys., Plasmas, Fluids, Relat. Interdisc. Top.* **2020**, *102*, 022803.

(26) Ruiz-Barragan, S.; Muñoz-Santiburcio, D.; Körning, S.; Marx, D. Quantifying Anisotropic Dielectric Response Properties of Nanoconfined Water within Graphene Slit Pores. *Phys. Chem. Chem. Phys.* **2020**, *22*, 10833.

(27) Motevaselian, M. H.; Aluru, N. R. Universal Reduction in Dielectric Response of Confined Fluids. *ACS Nano* **2020**, *14*, 12761−12770.

(28) Mondal, S.; Bagchi, B. Water Layer at Hydrophobic Surface: Electrically Dead but Dynamically Alive? *Nano Lett.* **2020**, *20*, 8959−8964.

(29) Monet, G.; Bresme, F.; Kornyshev, A.; Berthoumieux, H. Nonlocal Dielectric Response of Water in Nanoconfinement. *Phys. Rev. Lett.* **2021**, *126*, 216001.

(30) Kistler, S. F. In *Surfactant Science Series 49, Wettability*; Berg, J. C., Ed.; Marcel Dekker: New York, 1993; pp 311−429.

(31) Feng, J.; Guo, Z. Wettability of Graphene: from Influencing Factors and Reversible Conversions to Potential Applications. *Nanoscale Horiz.* **2019**, *4*, 339.

(32) Papadopoulou, E.; Megaridis, C. M.; Walther, J. H.; Koumoutsakos, P. Ultrafast Propulsion of Water Nanodroplets on Patterned Graphene. *ACS Nano* **2019**, *13*, 5465−5472.

(33) Zhang, C. Note: On the Dielectric Constant of Nanoconfined Water. *J. Chem. Phys.* **2018**, *148*, 156101.

(34) Esquivel-Sirvent, R. Anomaly of the Dielectric Function of Water under Confinement and Its Role in van der Waals Interactions. *Phys. Rev. E: Stat. Phys., Plasmas, Fluids, Relat. Interdiscip. Top.* **2020**, *102*, 042609.

(35) Neumann, M. Dipole Moment Fluctuation Formulas in Computer Simulations of Polar Systems. *Mol. Phys.* **1983**, *50*, 841−858.

(36) Kirkwood, J. G. The Dielectric Polarization of Polar Liquids. *J. Chem. Phys.* **1939**, *7*, 911−919.

(37) Raabe, G.; Sadus, R. J. Molecular Dynamics Simulation of the Dielectric Constant of Water: The Effect of Bond Flexibility. *J. Chem. Phys.* **2011**, *134*, 234501.

(38) Wu, Y.; Tepper, H. L.; Voth, G. A. Flexible Simple Point-Charge Water Model with Improved Liquid-State Properties. *J. Chem. Phys.* **2006**, *124*, 024503.

(39) Ballenegger, V.; Hansen, J. P. Dielectric Permittivity Profiles of Confined Polar Fluids. *J. Chem. Phys.* **2005**, *122*, 114711.

(40) Ghoufi, A.; Szymczyk, A.; Renou, R.; Ding, M. Calculation of Local Dielectric Permittivity of Confined Liquids from Spatial Dipolar Correlations. *EPL* **2012**, *99*, 37008.

(41) Schlaich, A.; Knapp, E. W.; Netz, R. R. Water Dielectric Effects in Planar Confinement. *Phys. Rev. Lett.* **2016**, *117*, 048001.

(42) Hamid, I.; Jalali, H.; Peeters, F. M.; Neek-Amal, M. Abnormal In-Plane Permittivity and Ferroelectricity of Confined Water: From Sub-Nanometer Channels to Bulk. *J. Chem. Phys.* **2021**, *154*, 114503.

(43) Lu, H.; Li, J.; Gong, X.; Wan, R.; Zeng, L.; Fang, H. Water Permeation and Wavelike Density Distributions inside Narrow Nanochannels. *Phys. Rev. B: Condens. Matter Mater. Phys.* **2008**, *77*, 174115.

(44) Fang, C.; Wu, X.; Yang, F.; Qiao, R. Flow of Quasi-Two Dimensional Water in Graphene Channels. *J. Chem. Phys.* **2018**, *148*, 064702.

(45) Kwon, S. S.; Choi, J.; Heiranian, M.; Kim, Y.; Chang, W. J.; Knapp, P. M.; Wang, M. C.; Kim, J. M.; Aluru, N. R.; Park, W. I.; Nam, S. Electrical Double Layer of Supported Atomically Thin Materials. *Nano Lett.* **2019**, *19*, 4588−4593.

(46) Duboué-Dijon, E.; Laage, D. Characterization of the Local Structure in Liquid Water by Various Order Parameters. *J. Phys. Chem. B* **2015**, *119*, 8406−8418.

(47) Breynaert, E.; Houlleberghs, M.; Radhakrishnan, S.; Grübel, G.; Taulelle, F.; Martens, J. A. Water as a Tuneable Solvent: A Perspective. *Chem. Soc. Rev.* **2020**, *49*, 2557−2569.

(48) Plimpton, S. Fast Parallel Algorithms for Short-Range Molecular Dynamics. *J. Comput. Phys.* **1995**, *117*, 1−19.

(49) Deserno, M.; Holm, C. How to Mesh up Ewald Sums. I. A Theoretical and Numerical Comparison of Various Particle Mesh Routines. *J. Chem. Phys.* **1998**, *109*, 7678−7693.

(50) Yeh, I. C.; Berkowitz, M. L. Ewald Summation for Systems with Slab Geometry. *J. Chem. Phys.* **1999**, *111*, 3155−3162.

(51) Werder, T.; Walther, J. H.; Jaffe, R. L.; Halicioglu, T.; Koumoutsakos, P. On the Water-Carbon Interaction for Use in Molecular Dynamics Simulations of Graphite and Carbon Nanotubes. *J. Phys. Chem. B* **2003**, *107*, 1345−1352.

(52) Fowkes, F. M.; Harkins, W. D. The State of Monolayers Adsorbed at the Interface Solid—Aqueous Solution. *J. Am. Chem. Soc.* **1940**, *62*, 3377−3386.

(53) Morcos, I. On Contact Angle and Dispersion Energy of the Cleavage Graphite/Water System. *J. Colloid Interface Sci.* **1970**, *34*, 469−471.

(54) Wang, S.; Zhang, Y.; Abidi, N.; Cabrales, L. Wettability and Surface Free Energy of Graphene Films. *Langmuir* **2009**, *25*, 11078−11081.

(55) Shin, Y. J.; Wang, Y.; Huang, H.; Kalon, G.; Wee, A. T. S.; Shen, Z.; Bhatia, C. S.; Yang, H. Surface-Energy Engineering of Graphene. *Langmuir* **2010**, *26*, 3798−3802.

(56) Schrader, M. E. Ultrahigh-Vacuum Techniques in the Measurement of Contact Angles. S. LEED Study of the Effect of Structure on the Wettability of Graphite. *J. Phys. Chem.* **1980**, *84*, 2774−2779.

(57) Li, Z.; Wang, Y.; Kozbial, A.; Shenoy, G.; Zhou, F.; McGinley, R.; Ireland, P.; Morganstein, B.; Kunkel, A.; Surwade, S. P.; Li, L.; Liu, H. Effect of Airborne Contaminants on the Wettability of Supported Graphene and Graphite. *Nat. Mater.* **2013**, *12*, 925−931.

(58) WCCNT. https://github.com/cselab/wccnt (accessed 2016-10-29).

(59) Humphrey, W.; Dalke, A.; Schulten, K. VMD − Visual Molecular Dynamics. *J. Mol. Graphics* **1996**, *14*, 33−38.